PNAS RESEARCH ARTICLE | MICROBIOLOGY

Control of biofilm formation by an *Agrobacterium tumefaciens* pterin-binding periplasmic protein conserved among diverse *Proteobacteria*

Jennifer L. Greenwich[a], Justin L. Eagan[a,1], Nathan Feirer[a,2], Kaleb Boswinkle[b,3], George Minasov[c,d], Ludmilla Shuvalova[e], Nicole L. Inniss[c,d], Jakka Raghavaiah[f,g], Arun K. Ghosh[f,g], Karla J. F. Satchell[c,d], Kylie D. Allen[b], and Clay Fuqua[a,4]

Affiliations are included on p. 9.

Edited by Susan Golden, University of California San Diego, La Jolla, CA; received November 18, 2023; accepted May 13, 2024

Biofilm formation and surface attachment in multiple Alphaproteobacteria is driven by unipolar polysaccharide (UPP) adhesins. The pathogen *Agrobacterium tumefaciens* produces a UPP adhesin, which is regulated by the intracellular second messenger cyclic diguanylate monophosphate (c-di-GMP). Prior studies revealed that DcpA, a diguanylate cyclase-phosphodiesterase, is crucial in control of UPP production and surface attachment. DcpA is regulated by PruR, a protein with distant similarity to enzymatic domains known to coordinate the molybdopterin cofactor (MoCo). Pterins are bicyclic nitrogen-rich compounds, several of which are produced via a nonessential branch of the folate biosynthesis pathway, distinct from MoCo. The pterin-binding protein PruR controls DcpA activity, fostering c-di-GMP breakdown and dampening its synthesis. Pterins are excreted, and we report here that PruR associates with these metabolites in the periplasm, promoting interaction with the DcpA periplasmic domain. The pteridine reductase PruA, which reduces specific dihydro-pterin molecules to their tetrahydro forms, imparts control over DcpA activity through PruR. Tetrahydromonapterin preferentially associates with PruR relative to other related pterins, and the PruR-DcpA interaction is decreased in a *pruA* mutant. PruR and DcpA are encoded in an operon with wide conservation among diverse Proteobacteria including mammalian pathogens. Crystal structures reveal that PruR and several orthologs adopt a conserved fold, with a pterin-specific binding cleft that coordinates the bicyclic pterin ring. These findings define a pterin-responsive regulatory mechanism that controls biofilm formation and related c-di-GMP-dependent phenotypes in *A. tumefaciens* and potentially acts more widely in multiple proteobacterial lineages.

biofilm | regulation | pterin | cyclic diguanylate monophosphate | protein structure

Significance

Biofilms are bacterial communities attached to surfaces, physiologically distinct from free-living cells, and a common cause of persistent infections. Here, we define the mechanism of a biofilm regulatory system based on excreted metabolites called pterins, that is conserved within a wide range of gram-negative bacteria, including multiple pathogens of animals and plants. The molecular mechanism of pterin-dependent regulation is reported including structural determination of several members of a family of pterin-binding proteins. Pterins are produced across all domains of life, and mechanistic insights into this regulatory circuit could lead to advances in antibiofilm treatments.

The regulation of bacterial attachment to surfaces plays a critical role in the formation of biofilms and can dictate their maturation. Biofilms are surface-associated microbial assemblages that are common among bacteria and result in dramatic physiological changes including substantial tolerance toward antibiotic treatment (1, 2). Biofilms act as protective reservoirs and thus represent a major challenge for the treatment of bacterial infections. Production of surface structures known as adhesins drives stable attachment of bacteria to surfaces, the first step in biofilm formation (3). Regulation of adhesin elaboration and activity thus can influence where and how biofilm formation occurs. In many bacteria, the transition from a free-living to a sessile mode of growth is under the regulatory control of the cytoplasmic second messenger cyclic diguanylate monophosphate (c-di-GMP). Increasing levels of c-di-GMP often promote attachment and biofilm formation through production of adhesive proteins and polysaccharides that drive the attachment process (4). Synthesis of c-di-GMP is catalyzed by diguanylate cyclases (DGCs), and its turnover is driven by phosphodiesterases (PDEs). Single bacterial taxa can have multiple DGCs and PDEs that influence the c-di-GMP pool, and multidomain proteins with dual DGC and PDE activities are not uncommon. Environmentally responsive modulation of c-di-GMP pools is mediated through control of gene expression and through allosteric regulation of these enzymes, many of which have sensory input modules. The flux of this second messenger in cells reflects the combined output of c-di-GMP synthesis and degradation activities (5).

The facultative plant pathogen, *Agrobacterium tumefaciens*, utilizes secreted polysaccharides to stably attach to biotic and abiotic surfaces, most prominently cellulose and a polar adhesin known as the unipolar polysaccharide (UPP) (6). *A. tumefaciens* is the causative agent of crown gall, a plant neoplastic disease that results from bacteria-to-plant horizontal gene transfer (7). Attaching to plant tissue is a requisite step in the virulence pathway of

Competing interest statement: K.J.F.S. has a significant interest in Situ Biosciences, a contract research organization that conducts research unrelated to this study. K.J.F.S. and her spouse are 100% owners of Situ Biosciences. All other authors declare no conflicts of interest.

This article is a PNAS Direct Submission.

[1]Present address: Department of Medical Microbiology and Immunology, University of Wisconsin, Madison, WI 53706.

[2]Present address: Department of Research and Development, Promega Corp., Madison, WI 53711.

[3]Present address: Department of Microbiology and Cell Science, University of Florida, Gainesville, FL 32603.

[4]To whom correspondence may be addressed. Email: cfuqua@indiana.edu.

This article contains supporting information online at https://www.pnas.org/lookup/suppl/doi:10.1073/pnas.2319903121/-/DCSupplemental.

Published June 13, 2024.

A. tumefaciens, but pathogenesis also involves additional plant-produced-signals to activate virulence (8). Production of the UPP, as well as cellulose, is under complex environmental control through c-di-GMP (9, 10). *A. tumefaciens* encodes close to 30 proteins with predicted DGC domains and only two solo PDE enzymes, but multiple proteins with predicted DGC domains also have PDE domains (6).

In our prior studies, we identified the DcpA protein, with both canonical DGC and PDE domains (9). DcpA has DGC and PDE activity in vivo, and genetic evidence suggests that both domains are functional. However, under standard laboratory conditions, DcpA is predominantly a PDE, maintaining low c-di-GMP levels and thereby limiting surface attachment. The N-terminal portion of DcpA has two transmembrane domains that flank an ~140 aa periplasmic domain. Our prior findings identified several other regulatory components critical for maintaining DcpA as a PDE. These additional regulators include the PruA pteridine reductase, which reduces certain 7,8-dihydropterins to their 5,6,7,8-tetrahydro forms (Fig. 1*A*), and PruR, a putative pterin-binding protein (9, 11). Both of these proteins are required to regulate the enzymatic activity of DcpA, and null mutants for *pruA* and *pruR* similarly lead to elevated c-di-GMP and aberrant activation of surface adhesion. The *pruR* gene is transcriptionally coupled with *dcpA* in a two-gene operon, consistent with their related functions.

Pterins are characterized by a nitrogen-rich, bicyclic ring structure with side chains of varying lengths and modifications extending from the ring carbon at the sixth position (Fig. 1*A*) (12). Well-known biomolecules with a pterin ring include the folates in which the side chain is composed of a para-amino benzoic acid group conjugated to a glutamic acid residue (or polyglutamate). Folate derivatives are required as cofactors for multiple aspects of one-carbon metabolism, and folate is essential in most organisms (13). More broadly, diverse pterin derivatives are found in all domains of life and in bacteria are known to act as enzymatic cofactors. Molybdopterin cofactor (MoCo) is a complex molybdenum-containing derivative used by various organisms as a prosthetic group to catalyze redox reactions. MoCo is synthesized from guanosine triphosphate (GTP) via a pathway that is independent from folate biosynthesis (14). Biopterin (BPt), neopterin (NPt) and monapterin (MPt) are pterins with hydroxylated 3 carbon side chains that function with cytoplasmic amino acid hydroxylases, but curiously the dominant fraction of these pterins is detected outside of cells (15). Pterins exist in a fully oxidized state as well as the reduced 7,8-dihydro and 5,6,7,8-tetrahydro states (Fig. 1*A*), the latter of which serves as the biologically active form of the respective cofactor. In *A. tumefaciens,* PruA catalyzes the NADPH-dependent reduction of H_2MPt to H_4MPt (11). Extracts of *A. tumefaciens* contain a methylated derivative of monapterin (2′-*O*-methylmonapterin) but this is undetectable in mutants with no PruA activity (9). Mutations that interfere with PruA activity result in high-level DGC activity from DcpA, driving elevated UPP-dependent adhesion.

The regulation of DcpA by PruA is indirect and requires PruR, but the mechanistic basis for this was undefined (9) (*SI Appendix*, Fig. S1*A*). PruR shares distant amino acid sequence similarity with sulfite oxidases and related enzymes, defined as the SUOX family, including YedY from *Escherichia coli* (16). SUOX proteins have domains that bind to MoCo to facilitate their enzymatic activities and have a conserved cysteine residue that coordinates the molybdenum atom in MoCo. There is no cysteine at this position in the PruR sequence and the protein has no predicted enzymatic activity (9, 17). Rather, we hypothesize that PruR is a pterin-binding protein functioning with non-MoCo pterin derivatives. Here, we report on the pterin-response mechanism, the structure of PruR, its control of DcpA, and conservation of this regulatory system in diverse *Proteobacteria*.

Results

PruR Regulates DcpA and Binds to Pterin Ligands In Vitro. The impact of elevated c-di-GMP on UPP and cellulose production can be qualitatively observed by cultivating *A. tumefaciens* derivatives on solid medium supplemented with the azo-dye Congo Red. Increased red pigmentation of colonies (the elevated Congo Red or ECR phenotype) is indicative of increased polysaccharide production (10). The ECR phenotype is also predictive for increased surface adhesion via the UPP. The *pruR* gene (ATU_RS16195) is encoded in an operon 9 bp immediately upstream of *dcpA* (ATU_RS16200). Our previous studies revealed that a precise in-frame deletion of the entire *pruR* coding sequence leads to a *dcpA*-dependent ECR phenotype and increased biofilm formation via elevated UPP production (9). We constructed a different deletion mutant, preserving potential translational coupling with *dcpA*, while deleting most of the *pruR* gene. This Δ*pruR* mutant exhibited a pronounced ECR phenotype and increased biofilm formation, and in contrast to our prior Δ*pruR* mutant, which impacted downstream *dcpA* expression (9), was well complemented with ectopic expression of *pruR* alone (*SI Appendix*, Fig. S1 *B* and *C*).

PruR was heterologously expressed and purified from *E. coli* to examine pterin binding in vitro. Based on our prior work showing the coordinated regulatory functions of PruR and the PruA pteridine reductase, we hypothesized that PruR would bind a tetrahydro-pterin produced by PruA (H_4MPt or H_4NPt) (9, 11). A restricted set of pterins are available commercially, and the tetrahydro forms are quite susceptible to oxidation. We synthesized an optically active H_2MPt from L-xylose by following a related reported procedure (18) and obtained dihydroneopterin (H_2NPt), dihydrofolate (H_2F), and tetrahydrofolate (H_4F) from commercial sources. H_4MPt and H_4NPt were generated enzymatically using *A. tumefaciens* PruA (11), where purified His_6-PruA was incubated with the dihydro-pterin substrates and NADPH, followed by addition of purified nontagged PruR under anaerobic conditions (*SI Appendix*, Fig. S2). Pterins bound to PruR were extracted and converted to their fully oxidized forms, which are stable and fluorescent. High performance liquid chromatography (HPLC) analysis indicated that PruR exhibits a higher affinity for H_4MPt compared to H_2MPt, as evidenced by higher levels of PruR-bound pterin observed in the PruA-coupled reaction compared to samples lacking PruA (Fig. 1*B* and *SI Appendix*, Fig. S3; *P*-value <0.05 compared to all other pterins). PruR also weakly associated with the neopterin derivatives but did not show a statistically significant preference for H_4NPt compared to H_2NPt (Fig. 1*B*). Low levels of folate were recovered from PruR in binding experiments with H_2F and H_4F, which were significantly less than the amount of pterin observed in experiments with H_4MPt and H_4NPt (Fig. 1*B*).

PruR Actively Modulates the DGC and PDE Activity of DcpA. The in vivo phenotypes of several *dcpA* point mutants suggested that it has both DGC and PDE activity, but that the PDE activity is dominant in planktonic laboratory culture (9, 10). Enzymatic assays of the purified DcpA cytoplasmic domain (res. 190 to 644, see *Materials and Methods*) revealed that the protein has both activities (*SI Appendix*, Fig. S4), although the DGC activity is weaker (0.26 A_{360} units $min^{-1}mol^{-1}$) compared to PDE activity (15.7 A_{360} units min^{-1} mol^{-1}). It was unclear however whether the PruR-dependent PDE-dominant activity of DcpA in vivo reflects PruR stimulation of the PDE activity, the inhibition of DGC activity, or both.

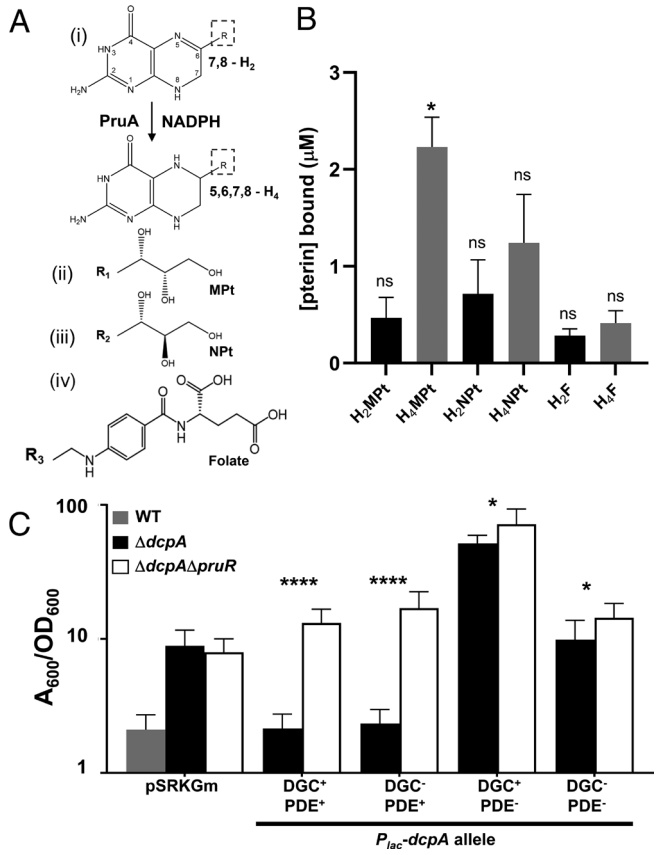

Fig. 1. PruR binds pterins and is required to control both the DGC and PDE activity of DcpA. (*A*) PruA reaction and relevant pterin molecule structures. i): PruA uses NADPH as a cofactor and catalyzes the reduction of a 7,8-dihydropterin substrate to a 5,6,7,8-tetrahydropterin. Atoms are numbered in the dihydropterin. R indicates side groups as shown in (ii)–(iv): ii): R1—monapterin; iii): R2—neopterin; and iv): R3—*p*ABA-glutamate (folate). (*B*) In vitro pterin binding assays were performed as described in supplemental methods with purified Δ_{SS}-PruR (50 μM), NADPH, and with or without His_6-PruA. HPLC fractioned reactions were examined by fluorescence for the oxidized pterins (excitation: 356 nm; emission: 450 nm). UV absorbance at 283 nm was used to measure folate relative to standards. PruR was incubated with the following pterin or folate species: H_2MPt, dihydromonapterin; H_4MPt, PruA-generated-tetrahydromonapterin; H_2NPt, dihydroneopterin; H_4NPt, PruA-generated tetrahydroneopterin; H_2F, dihydrofolate; and H_4F, tetrahydrofolate. Bars are averages of triplicate assays with error bars as SD and analyzed by standard one-way ANOVA and post hoc Tukey analysis (*P* values relative to H_4MPt, *, <0.05, ns, not significant). (*C*) Biofilm assays of the *A. tumefaciens* C58 wild type (WT, gray bar), a Δ*dcpA* mutant (black bars), or a Δ*dcpA*Δ*pruR* double mutant (white bars) containing the vector control or a plasmid-borne P_{lac}-*dcpA* fusion induced with 500 μM isopropyl β D 1-thiogalactopyranoside (IPTG) expressing either the wild-type *dcpA* or catalytic site mutants (DGC^-, E308A; PDE^-, E431A; DGC^-PDE^-, both). The ratio of acetic acid–solubilized CV absorbance (A_{600}) from 48 h biofilm assays normalized to the OD_{600} planktonic turbidity from the same culture. Assays were performed in triplicate and error bars are SD; *P* values calculated comparing complementation of *dcpA* in the Δ*dcpA* strain compared to the Δ*dcpA*Δ*pruR* strain by standard two-tailed *t* test. (*P* values, * <0.05, **** <0.0001)

Ectopic expression of *dcpA* alone in *E. coli*, in the absence of *pruR*, resulted in high-level c-di-GMP synthesis and mutation of the DGC catalytic motif (GGDEF>GGDAF; E308A) abolished this c-di-GMP increase, suggesting that PruR is required for dominant PDE activity (9). Plasmid-borne expression of wild-type *dcpA* complements the elevated biofilm formation of *the* Δ*dcpA* mutant to normal levels (Fig. 1*C*). By contrast, the Δ*pruR*Δ*dcpA* mutant harboring this plasmid exhibits a dramatic increase in biofilm formation relative to the wild type, and higher than the single *dcpA* mutant, consistent with the increased c-di-GMP caused by *dcpA* ectopic expression in a *pruR* null mutant (9). Expression of the $DGC^-(PDE^+)$ $DcpA_{E308A}$ allele in the Δ*dcpA* mutant decreases biofilm formation to wild-type levels. However, this allele fails to cause this decrease in the Δ*pruR*Δ*dcpA* mutant, suggesting that PDE activity is under PruR control. Ectopic expression of *dcpA* in the wild type does not significantly diminish biofilm formation (likely due to c-di-GMP production by other DGCs) (9).

In the absence of PruR, the PDE activity of DcpA is not increased by ectopic expression of DcpA. Mutation of *dcpA* to abolish DcpA PDE activity (EAL>AAL; E431A; PDE^-DGC^+) resulted in striking stimulation of biofilm formation when this mutant is ectopically expressed in the Δ*dcpA* mutant (Fig. 1*C*). However, expression of the $DcpA_{E431A}$ allele in the Δ*pruR*Δ*dcpA* mutant imparts even more dramatic biofilm stimulation, suggesting that PruR dampens DGC activity in addition to stimulating PDE activity, and its effects on these two activities are genetically separable. Ectopically expressing an allele mutated for both domains (DGC^-PDE^-, E308A E431A) does not strongly impact biofilm formation in either the Δ*dcpA* or the Δ*pruR*Δ*dcpA* mutant but shows a slight increase in the *pruR-dcpA* double mutant relative to the Δ*dcpA* mutant.

PruR Is Secreted and Active in the Periplasm. Sequence analysis suggests that the PruR protein has an N-terminal secretion signal (aa 1 to 22, Signal-P score 0.31, Fig. 2*A*). Given our hypothesis that PruR is a pterin-binding protein, this prediction is surprising, as the only established function of bacterial pterins is to serve as cofactors for amino acid hydroxylases, which are cytoplasmic enzymes (15). To experimentally evaluate whether PruR is secreted to the periplasm in vivo, we first tested this genetically by fusing it to *phoA*, encoding the enzyme alkaline phosphatase (AP) that requires periplasmic localization for activity (19). Plasmid-borne, ectopic expression of the *pruR-phoA* fusion in *A. tumefaciens* led to detectable AP activity in whole cells, above the very low levels of the same strain lacking *phoA* (*SI Appendix*, Fig. S5*A*). Furthermore, fusion of only the *pruR* signal sequence (res. 1 to 22) with *phoA* ($pruR_{SS}$-*phoA*) similarly expressed from the same plasmid resulted in much stronger AP activity. Neither construct was affected by expression in the Δ*pruR* null mutant. It is likely that the full-length PruR-PhoA fusion partially diminishes AP activity.

The periplasmic localization of PruR was tested directly by separating wild-type *A. tumefaciens* cells and several derivatives into periplasmic and cytoplasmic fractions using an osmotic shock protocol and probing western blots with a polyclonal antibody preparation raised against PruR (α–PruR). Wild-type cells clearly revealed a protein the size of the processed form of PruR (146 aa, predicted 16.1 kDa) in the periplasmic fraction, whereas a Δ*pruR* mutant lacked this protein (Fig. 2*B*). Ectopic expression of a plasmid-borne copy of *pruR* expressed from P_{lac} in the Δ*pruR* mutant revealed an IPTG-inducible PruR protein in the periplasmic fraction. In contrast, the same expression construct deleted for the *pruR* signal sequence (Δ_{SS}*pruR*) results in PruR that remains in the cytoplasmic fraction.

Complementation of a Δ*pruR* mutant (a mutation which is partially polar on *dcpA*) with a plasmid expressing *pruR* and *dcpA* rescues this mutant to normal levels of surface attachment (Fig. 2*C*). However, expression of the same plasmid expressing the Δ_{ss}*pruR* allele and *dcpA* failed to rescue these phenotypes (Fig. 2*C*). The even greater surface adherence observed with the (P_{lac}-Δ_{ss}*pruR-dcpA*) plasmid was most likely due to its additional copy of *dcpA*.

Although PruR has a match for an N-terminal signal sequence, there was a stronger match identified for a lipidation site in the signal sequence predicted at cysteine 19 (C19, Signal-P score 0.68, Fig. 2*A*) (20). In this analysis, PruR would be lipidated at C19

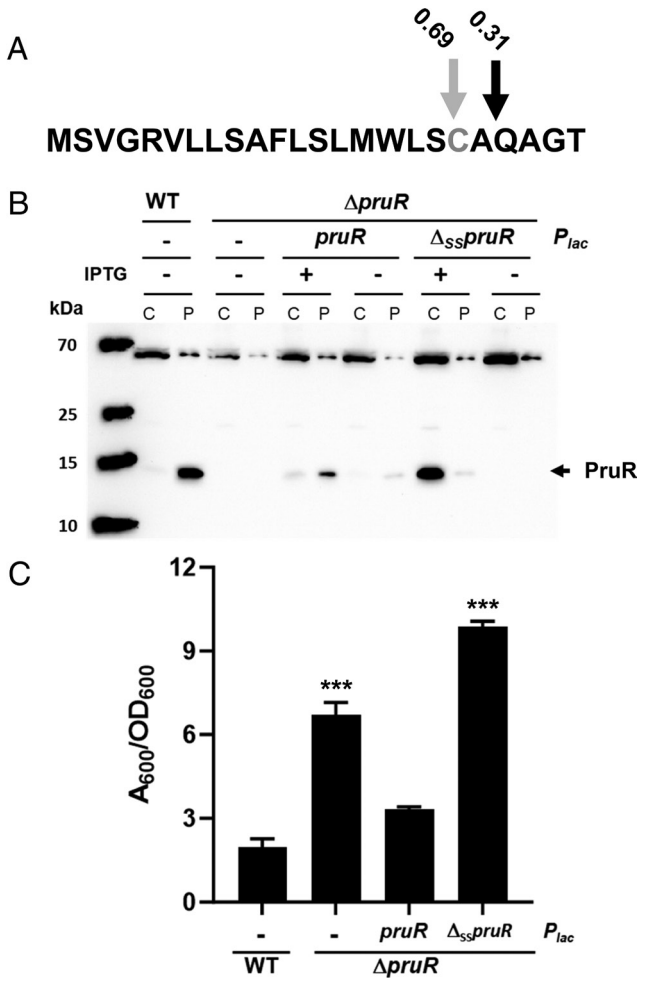

Fig. 2. PruR is a periplasmic protein. (*A*) Signal P prediction of the PruR N-terminal signal sequence. Black arrow, predicted signal peptidase cleavage site; gray arrow, putative cleavage and lipidation site; gray text, predicted lipidated Cys19. (*B*) Western blot of Sodium dodecylsulfate polyacrylamide gel electrophoresis (SDS-PAGE) using α-PruR polyclonal antisera to probe extracts of wild-type *A. tumefaciens* C58 WT and the Δ*pruR* mutant on its own or expressing either the P_{lac}-*pruR* plasmid or the P_{lac}-Δ_{SS}*pruR* plasmid (both plasmids also expressing *dcpA*). Cultures were grown to similar densities with or without induction with 400 μM IPTG and fractionated to separate the cytoplasmic/membrane fraction (C lanes) from the periplasmic fraction (P lanes). Antibody binding was detected with goat anti-rabbit secondary antibody conjugated to horseradish peroxidase (GAR-HRP) and chemiluminescentsubstrate exposed on a BioRad ChemiDoc. (*C*) Biofilm assays of WT or a Δ*pruR* mutant derivative with the empty vector plasmid (−) or harboring a plasmid-borne P_{lac} fusion expressing either *pruR* or Δ_{SS}*pruR* (both plasmids also express *dcpA*). Ratio of acetic acid-solubilized CV A_{600} from 48 h biofilm assays normalized to the OD_{600} planktonic turbidity of the same culture. Assays performed in triplicate and error bars are SD; *P* values calculated by standard two-tailed *t* test (*P* values, *** <0.01).

with signal peptidase cleavage between it and the adjacent serine at position 18 (S18, Fig. 2*A*), rather than A22 as predicted for the nonlipidated secretion signal. Lipidated PruR would be predicted to associate with the periplasmic leaflet of the inner membrane rather than the outer membrane (21). Although this predicted lipidation site is an imperfect match to the spacing for the canonical sequence "lipobox" motif (L[A/S][A/G]C), we tested whether C19 is required for PruR activity. Ectopic expression of a *pruR* allele with this cysteine residue mutated to an alanine (C19A) fully complemented the elevated biofilm phenotype of the Δ*pruR* mutant, suggesting that PruR is not lipidated, or minimally that it does not have to be anchored to the inner membrane to function in the periplasm (*SI Appendix*, Fig. S5*B*). Furthermore, *pruR* was effectively secreted and retained full activity when fused with the *malE* and *dsbA* signal sequences ($MalE_{SS}$ and $DsbA_{SS}$) from *E. coli*, well characterized to direct two distinct Sec-dependent secretion mechanisms, and to be nonlipidated (22, 23) (*SI Appendix*, Fig. S5 *C* and *D*).

In Vivo Cross-Linking Reveals a PruR-DcpA Complex. Direct interaction of PruR with the periplasmic region of DcpA would be one mechanism by which pterins could regulate DcpA DGC and PDE activity. To test this hypothesis, we used disuccinimidyl suberate (DSS) to perform protein cross-linking with cell suspensions of *A. tumefaciens* and then probed for PruR and DcpA proteins using polyclonal antibodies against PruR (α-PruR) and separately to the periplasmic portion of DcpA (Fig. 3). The PruR protein is ~16 kDa, and full-length DcpA is ~70 kDa. Upon DSS addition in wild-type cells, SDS-PAGE separation, and western blotting with α-PruR antibody, an additional protein species of ~85 kDa is observed (Fig. 3*A*). This species is absent in Δ*dcpA* and Δ*pruR* mutants but is significantly more pronounced in

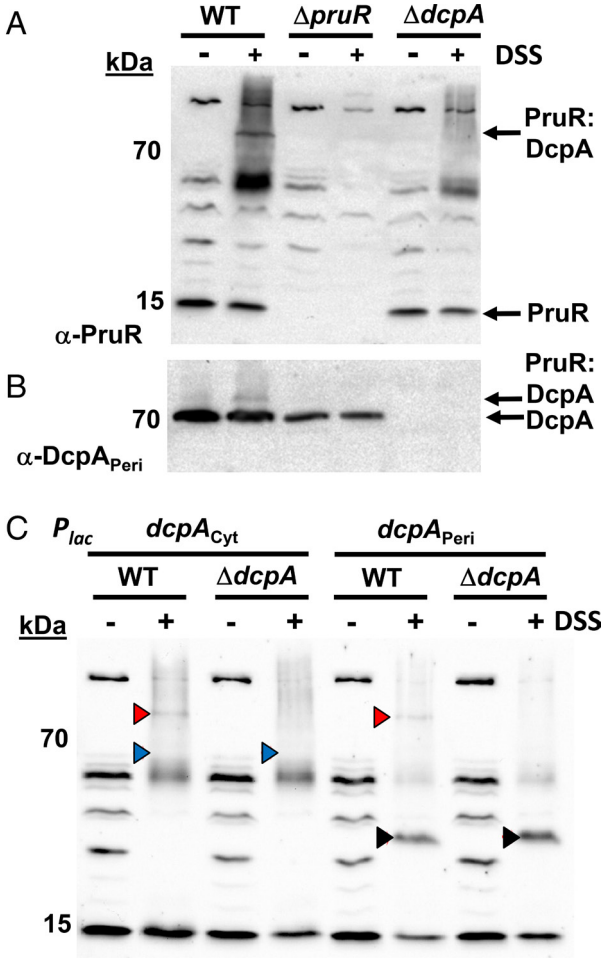

Fig. 3. PruR forms a complex with the periplasmic region of DcpA. Western blots with whole cell suspensions that were either untreated or incubated with DSS cross-linker (0.75 mM) and separated on 10% SDS-PAGE gels. Antibody binding was detected with GAR-HRP secondary antibody and chemiluminescent substrate exposed on a BioRad ChemiDoc. Nonspecific bands serve as protein loading controls. (*A* and *B*) Cell suspensions were prepared from *A. tumefaciens* mutants deleted for the cellulose operon to reduce clumping (Δ*cel*); with Δ*cel*Δ*pruR* and Δ*cel*Δ*dcpA* mutants (*C*) Wild-type *A. tumefaciens* or Δ*dcpA* ectopically expressing the cytoplasmic ($DcpA_{cyt}$) or periplasmic ($DcpA_{peri}$) domains of DcpA from P_{lac}. Antibodies were α-PruR polyclonal antibody (1:40,000 dilution) and α-$DcpA_{Peri}$ (1:20,000 dilution). 400 μM IPTG was added to induce P_{lac}. Complexes are indicated as labeled, PruR-DcpA, 87 kDa; DcpA, 71 kDa; PruR; 16 kDa. Red, blue, and black triangles in panel *C* indicate the full-length DcpA-PruR complex, the expected size of the PruR-$DcpA_{cyt}$ complex (~66.5 kDa), and the PruR-$DcpA_{peri}$ complex (~37.8 kDa), respectively.

wild-type *A. tumefaciens* expressing the P_{lac}-*pruR-dcpA* construct (*SI Appendix*, Fig. S6*A*). Probing these western blots with a lower titer α-DcpA antibody preparation against the periplasmic domain captured the complex in wild-type cells (Fig. 3*B*) and those harboring the P_{lac}-*pruR-dcpA* plasmid (*SI Appendix*, Fig. S6*B*), but not the Δ*pruR* or Δ*dcpA* mutants.

Next, we tested the interaction of PruR independently with the periplasmic and cytoplasmic DcpA domains. The DcpA periplasmic domain including its two transmembrane elements (expressing codons 1 to 192) and the DcpA cytoplasmic region (codons 190 to 644) were independently expressed from P_{lac} either in the wild type or the Δ*dcpA* mutant. DSS cross-linking of whole cell suspensions revealed efficient PruR cross-linking with the DcpA periplasmic domain (predicted ~37.4 kDa cross-linked complex) but not with the cytoplasmic domain (predicted 66.5 kDa complex) (Fig. 3*C*). In the wild-type background, the full-length PruR-DcpA complex was also visible, when probed for either PruR or the periplasmic domain of DcpA, but this was abolished in the Δ*dcpA* mutant. These results are consistent with the genetic evidence that the PruR-DcpA interaction occurs in the periplasm.

PruR Interaction with the DcpA Periplasmic Domain Is Decreased in a *pruA* Mutant. The Δ*pruA* mutant manifests a dramatic increase in UPP production and surface attachment, similar to mutants of *pruR* or *dcpA*, and its impact is dependent on the presence of functional *dcpA* and *pruR* genes (9). To evaluate whether reduced pterin species generated by PruA impact PruR-DcpA interactions, we compared DSS cross-linking for whole cell suspensions of the Δ*pruA* mutant compared to the wild type, both ectopically expressing PruR and the periplasmic domain of DcpA (these derivatives retain the chromosomal *pruR-dcpA* genes). The amount of complex formation between PruR and $DcpA_{Peri}$ was substantially diminished in the Δ*pruA* mutant relative to the wild type using both the α–PruR (Fig. 4*A*) and α–$DcpA_{Peri}$ (Fig. 4*B*) antibodies (multiple repeats presented in *SI Appendix*, Fig. S6 *C–E*). The amount of uncomplexed PruR was also somewhat decreased, suggestive of destabilization in the periplasm. Overall these results reveal that *pruA* is required for maximal complex formation between PruR and DcpA, suggesting that pterins formed by PruA foster the PruR-DcpA interaction.

Conservation of *pruR-dcpA*-Type Operons among Proteobacteria. Well-conserved homologs of PruR exist in multiple proteobacterial taxa (Fig. 5*A*). These proteins are of similar sizes with an N-terminal secretion signal and conserved residues common among the SUOX family of proteins (see residues marked by asterisks in *SI Appendix*, Fig. S7*A*). Notably, all lack the critical cysteine involved in MoCo binding in SUOX proteins and instead have a tryptophan. Inspection of the genomic location for the *pruR* homologs in these proteobacteria reveals presumptive bicistronic operons with a downstream gene encoding a DcpA homolog which is composed of two transmembrane domains flanking a periplasmic loop and a large cytoplasmic portion of the protein. Many of these have both DGC and PDE domains such as DcpA, although in some cases, they have only the DGC domain without the C-terminal PDE (Fig. 5*A* and Dataset S1). The predicted periplasmic domains of these *dcpA* homologs are roughly the same length (138 to 150 aa) and show overall chemically similar residues with two invariant positions in common, a tryptophan and a glutamate (WX_7E; W40 and E48, in the full-length *A. tumefaciens* DcpA) (*SI Appendix*, Fig. S7*B*).

Higher resolution iterative searching of bacterial genomes using a Hidden Markov Model (*Materials and Methods*) for *pruR* homologs with adjacent genes encoding proteins with a periplasmic domain similar to DcpA revealed over 5,500 unique regulatory

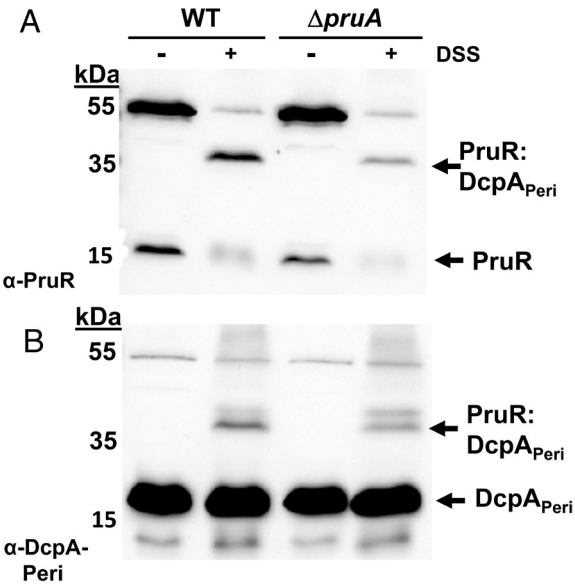

Fig. 4. Deletion of *pruA* diminishes the interaction between DcpA and PruR. Western blot probing for the PruR-$DcpA_{peri}$ complex following in vivo DSS cross-linking in the *A. tumefaciens* wild type or a Δ*pruA* mutant expressing the P_{lac}-*pruR-dcpA*$_{peri}$ plasmid (400 μM IPTG). Probed with polyclonal antibody preparations (*A*) α-PruR, 1:40,000; (*B*) α-$DcpA_{peri}$, 1:20,000. Antibody binding was detected with GAR-HRP secondary antibody and a chemiluminescent substrate on a BioRad ChemiDoc. Nonspecific bands serve as protein loading controls.

pairs among *Proteobacteria* of Alpha (APB), Beta (BPB), Gamma (GBP), and Delta (DBP) classes (Fig. 5*B* and Dataset S1). The distribution of these regulatory genes is nonuniform within specific families and genera, with single bacterial taxa encoding as many as four discrete regulatory pairs (Dataset S1). Roughly 77% of the genes linked to *pruR* encode DGC domains, many with a C-terminal PDE domain such as with DcpA (Fig. 5*A*). In 23% of the gene pairs meeting the search criteria, the cytoplasmic domain is not related to c-di-GMP, but rather is composed of a two-component-type sensor kinase domain similar to TorS and BaeS (25, 26), often with a PAS domain and/or a response regulator domain (Fig. 5*B* and *SI Appendix*, Fig. S8). We tentatively designate these gene clusters as PruR-DTB (DcpA-periplasmic domain - TorS/BaeS cytoplasmic domain) systems.

PruR-Type Proteins Share a Common Structural Fold. Based on our experimental findings for PruR-pterin interactions and on sequence conservation, we hypothesized that PruR represents a class of proteins with an overall fold similar to the MoCo-binding domains of SUOX-type proteins, that instead bind to the non-MoCo pterins. We purified representative members of the PruR family and determined their three-dimensional structures by X-ray crystallography (*SI Appendix*, Tables S1 and S2). The *A. tumefaciens* PruR structure reveals a general structural motif composed of ten β-sheets and seven α-helices (Fig. 6*A*, PDB 7kou, 1.5 Å). The β-strands form one mixed, five-stranded β sheet (2-1-10-5-6) and one curved, four-stranded antiparallel β-sheet (3-4-7-9), and these sheets are interconnected by short α helices (1, 2, 3, 5, 6, and 7). We solved an additional crystal structure of *A. tumefaciens* PruR (PDB 7kos) for which the overall structure is identical except that in this crystal form a small surface pocket is occupied by the side chain residues of neighboring or symmetry-related polypeptide chains (*SI Appendix*, Fig. S9 and Table S1).

Structures of three other PruR homologs were also solved including proteins from *V. vulnificus* (PDB 7kom, 30% identity; 1 Å), *Vibrio cholerae* (PDB 7kp2, 32% identity, 1.03 Å), and *Klebsiella pneumoniae* (PDB 7rkb, 59% identity, 2.5 Å) (Fig. 6 *B*

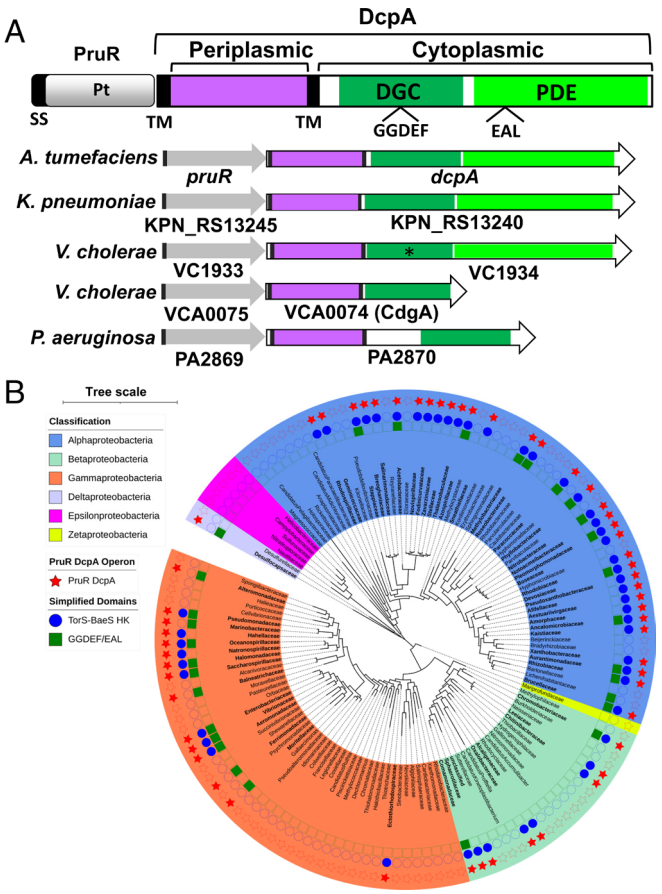

Fig. 5. The *pruR-dcpA* operon is conserved across multiple Proteobacteria. (*A*) Domain structure for PruR and DcpA; transmembrane domains and signal sequence are black lines; the DcpA periplasmic domain is purple; the DGC domain is green; the PDE domain is lime green; Pt indicates the pterin-binding activity of the protein. The arrow diagrams indicate presumptive operon structure for homologs of the *pruR-dcpA* operon from multiple pathogens. A subset of DcpA homologs are truncated relative to DcpA and contain only the DGC domain, and degenerate DGC domains predicted to be catalytically inactive are marked with an asterisk. *Klebsiella pneumoniae pneumoniae* ATCC 700721; *Vibrio cholerae,* O1 biovar El Tor str. N16961*; Vibrio vulnificus* CMCP6; *Pseudomonas aeruginosa* PA01. Gene and domain sizes are proportional. (*B*) Radial phylogram of APB, BBP, DBP, EBP, and GMP representing bacterial families. Bolded family names and red stars indicate taxa with *pruR* genes linked with a *dcpA*-periplasmic domain. Green and blue dots indicate a PruR linked to a DcpA-periplasmic domain with a GGDEF/EAL (PruR-DcpA) or a TorS-BaeS HK (PruR-DTB) cytoplasmic domain, respectively. Tree was generated using Interactive Tree of Life (24).

and *C*). Multiple sequence and structure alignments of these PruR homologs clearly show that the structures are highly similar (rmsd of 0.6 to 2.0 Å) and all share the SUOX-like fold.

PruR Has a Truncated MoCo-Binding Site that Associates with a Pterin. Structural comparison of *A. tumefaciens* PruR to chicken liver sulfite oxidase (PDB 1sox), a relatively close SUOX structural homolog, and *E. coli* YedY (PDB 1xdq), a more distant sequence homolog (27), revealed significant structural overlap with the MoCo-binding domains (Fig. 7 *A* and *B*). PruR from *A. tumefaciens* aligns well over 126 aa residues with the chicken liver SUOX protein (rmsd of 2.5 Å) and over 125 residues with *E. coli* YedY (rmsd 2.3 Å) (*SI Appendix*, Fig. S10*A*). The binding sites of chicken liver SUOX and *E. coli* YedY contain a single molybdopterin bound to a surface cleft characterized by the conserved cysteine residue at the end of a lengthy β-hairpin (Fig. 7 *A* and *B*, *Left*). Although the overall MoCo-binding fold is well-aligned between these proteins, PruR appears to lack a deep binding cleft in the region that could accommodate MoCo, and the β-hairpin with the conserved cysteine residue in all SUOX proteins, including in *E. coli* YedY (res. 98 to 109), is truncated in PruR (res. 66 to 74) (Fig. 7 *A* and *B*). Furthermore, structural-sequence alignments of PruR, YedY, and chicken liver sulfite oxidase show that the canonical molybdenum-coordinating cysteine is substituted with a tryptophan (W70) in PruR, which constitutes a proline-tryptophan (^{69}PW^{70}) motif conserved in most PruR homologs (Fig. 6*C* and *SI Appendix*, Fig. S7*A*). Thus, the PruR fold is like that of SUOX family MoCo-binding domains but several structural determinants for MoCo binding, including a longer binding cleft, are lacking. The shorter pocket identified in our structures, however, can accommodate a smaller non-MoCo pterin molecule.

To examine the pterin-PruR interaction, we cocrystallized PruR with H_2NPt, a commercially available monapterin stereoisomer that is more stable to oxidation than the tetrahydro pterins and thus compatible with crystallization methods. We obtained the ligand-bound structures for both *K. pneumoniae* and *V. cholerae* PruR homologs (7rkb and 7kp2, respectively) (*SI Appendix*, Table S1). Refinement revealed both were bound by the bicyclic moiety of the neopterin, with the hydroxylated tail absent. In all structures, the neopterin ring is positioned in the pterin-binding cleft and is sandwiched between a tyrosine and tryptophan (*A. tumefaciens* Y104 and W160, respectively) (Fig. 7*C*). The pterin also forms hydrogen bonds with an asparagine residue (N102). These three residues are well conserved among PruR homologs (Fig. 6*C*), and Y104 is conserved in other SUOX proteins including YedY (*SI Appendix*, Fig. S10*B*). Notably, in our apo structure of *A. tumefaciens* PruR, the Y104 side chain is flipped away from the pterin-binding pocket (Fig. 7*C*), suggesting that binding of a ligand to this cleft induces key stacking interactions that stabilize the pterin in the site. Further comparison of the pterin-bound PruR structures also revealed three alternative binding conformations of neopterin. The orientation of the ring moiety varies, yielding different positions of the hydroxylated tail (Fig. 7*D* and *SI Appendix*, Fig. S11 *A–C*). The observed variation in binding modes of neopterin may be due to differences between this disfavored fully oxidized ligand and the more reduced cognate pterin species (9). Individual site-specific mutations of the conserved residues that form the presumptive pterin-binding site in *A. tumefaciens* PruR (LN102AA, Y104A, W160A) decrease the ability of ectopically expressed *pruR* to complement the Δ*pruR* mutant for its ECR and elevated adherence phenotypes (Fig. 7*E* and *SI Appendix*, Fig. S10*C*), and these mutants are less efficiently cross-linked to DcpA when expressed in *A. tumefaciens* (Fig. 7*F*).

Discussion

Here, we describe the regulation of the dual-function DGC/PDE DcpA by a pterin-binding protein PruR, building from our previous findings (9–11). All three components of the pterin regulatory pathway discussed here (PruR, DcpA, and PruA) were identified in a transposon mutagenesis screen designed to identify regulators of surface attachment in *A. tumefaciens* (10). In this study, we have further interrogated the pterin regulatory mechanisms that function in this pathway. In so doing, we determined the three-dimensional structure of PruR and selected homologs in their apo forms, and two in complex with a pterin. We have also revealed a wide distribution of the PruR-DcpA-type regulators among the *Proteobacteria*, and their similarity suggests that they are likely to also utilize pterin-dependent regulation.

An Emergent Class of Pterin-Binding Proteins. The overall fold of pterin-binding PruR-type proteins suggests that they are a branch of the SUOX protein family, cytoplasmic enzymes including sulfite

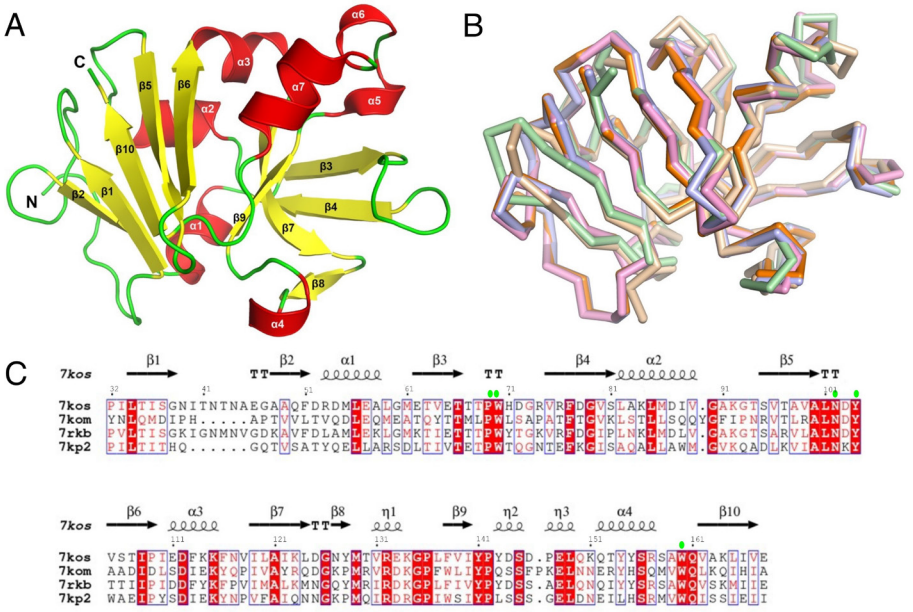

Fig. 6. The structure of PruR is conserved in multiple Alpha- and Gammaproteobacteria. (*A*) The overall structure of PruR from *A. tumefaciens* (7kos) is depicted. The secondary structure elements are labeled and shown in red (α helices), yellow (β-strands), and green (loops). (*B*) Superpositions are presented of PruR from *A. tumefaciens* (orange, 7kos; violet, 7kou), *K. pneumoniae* (pink, 7rkb) *V. cholerae* (wheat, 7kp2), *V. vulnificus* (light green, 7kom). The peptide main chains of all structures are depicted as ribbons. (*C*) Multiple sequence alignments are presented for PruR proteins from *A. tumefaciens* (At 7kos), *K. pneumoniae* (Kp 7rkb) *V. cholerae* (Vc 7kp2), *V. vulnificus* (Vv 7kom) with secondary structure elements from At PruR mapped above. The lime green circles mark pterin-binding site residues conserved across all proteins.

oxidases and nitrate reductases that utilize MoCo as a cofactor (16). Most SUOX proteins have additional domains that drive catalysis. In contrast, PruR-like proteins are small, almost entirely composed of the SUOX fold and their N-terminal secretion signal. Consistent with these differences, the PruR-bound pterins such as H_4MPt and related molecules are significantly smaller and less structurally complex than MoCo. It is intriguing that the pterin-binding site for PruR-type proteins and the SUOX MoCo-binding site are structurally and likely evolutionarily related, especially given the markedly different functions of the two groups of proteins.

Other proteins that bind pterins are the aromatic amino acid hydroxylases such as phenylalanine hydroxylase (PAH), which coordinates tetrahydrobiopterin (H_4BPt) as a cofactor. The pterin-binding site contains an iron atom and a conserved acidic residue that coordinates the pteridine ring through water-mediated interactions (28). This binding site thus bears no significant similarity to the SUOX-type pterin-binding site of the PruR-type proteins we define here. There are also well-studied, membrane-anchored mammalian proteins that associate with the essential metabolite folate, which also contains the bicyclic pteridine ring. These folate-binding proteins are up-regulated in fetal cells and certain cancers (29, 30), and dramatically alter their conformation upon binding to folate. Similar to PruR-like proteins, their association with the pteridine ring in folate is fostered by conserved Tyr and Trp residues that sandwich the ring in a hydrophobic pocket, although these proteins are otherwise structurally distinct from the PruR-type proteins reported here.

Preference of PruR for Fully Reduced Monapterin. The pterin binding specificity of PruR was revealed by in vitro studies with purified PruR and different pterin species. Fully reduced tetrahydropterins oxidize readily to the dihydropterin forms (31), which makes in vitro binding experiments more challenging. We used PruA pteridine reductase and NADPH in the presence of H_2MPt and H_2NPt under anoxic conditions to generate the respective tetrahydropterin species in the presence of PruR (11). PruA-reduced H_4MPt bound to PruR more efficiently than the H_2MPt, whereas the NPt and folate ligands bound more weakly, with no significant impact of the reduced tetrahydro derivatives. Although this experiment provides robust evidence for the pterin association with PruR, it does not provide binding affinities.

Cocrystallization with H_2NPt and the PruR homologs from *V. cholerae* (7kou) and *K. pneumoniae* (7rkb) revealed the fully oxidized neopterin (presumably due to oxidation of the exogenously added H_2NPt during crystallization) binding a location analogous to the MoCo-binding site on SUOX. Pterin binding occurs within the pterin-binding cleft we have defined on PruR-type proteins through interaction of the pteridine ring sandwiched between the conserved tyrosine (Y014)and tryptophan (W160) residues, and hydrogen bonding through the conserved asparagine (N102) and several other hydrogen bonding positions. The hydroxylated tail of the neopterin was not visible in these structures suggesting it was disordered. The stereochemistry of the hydroxylated tail distinguishes monapterin from its stereoisomer neopterin, and the more complex benzoyl and glutamyl side chain substituents of folate, and we hypothesize that interactions between this tail and PruR add binding specificity. Additionally, the binding site may also interact directly with the fully reduced tetrahydropterin species through interactions that are not observed in the crystal structures with oxidized neopterin. The multiple orientations of the neopterin detected within the binding cleft may also reflect weaker interactions of the protein with the noncognate, fully oxidized neopterin molecule. Mutation of several of the conserved residues that comprise the pterin-binding site impact the interaction with DcpA and its downstream regulatory outputs, validating the importance of this binding site in pterin-responsive control.

PruR Interacts with Pterins in the Periplasm. The best-studied functions for bacterial pterins are to act as enzymatic cofactors for amino acid hydroxylase enzymes such as PAH (15). All evidence suggests that PruA drives reduction of H_2MPt in the cytoplasm, but our findings have revealed that PruR functions and responds to pterins in the periplasm. A longstanding, unexplained observation among

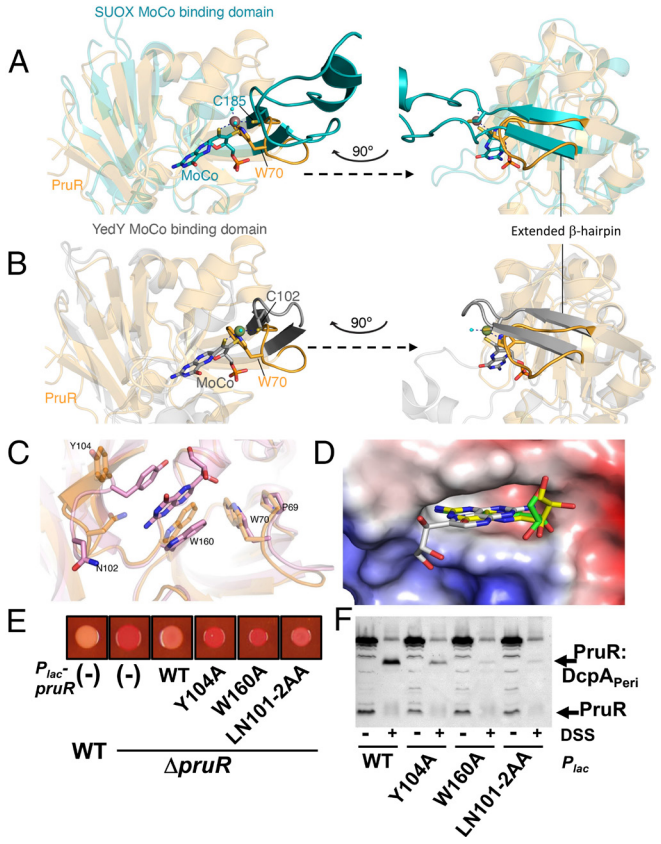

Fig. 7. The PruR structure is a degenerate SUOX fold and PruR binds pterins. Superposition of *A. tumefaciens* PruR (orange, 7kou) with the MoCo-binding domain of (*A*) chicken liver SUOX (teal, PDB 1sox) and (*B*) *E. coli* YedY (gray, PDB 1xdq). The structures are depicted as transparent cartoons, except for key determinants of the MoCo-binding region, which are opaque (see *SI Appendix*, Fig. S10*A* for full structure comparisons). The MoCo and conserved Cys185 of SUOX and Cys102 of YedY are shown as balls-and-sticks (carbon, teal or gray; oxygen, red; nitrogen, dark blue; sulfur, yellow), the molybdenum is shown as a mauve or olive sphere for SUOX and YedY, respectively, water molecules as small cyan spheres, and hydrogen bonds as navy, dashed lines. W70, conserved in PruR, is also shown as sticks. Structures in images on the left were rotated 90° around the *y*-axis toward the viewer to obtain images on the right (as indicated by dashed arrows) where the extended β-hairpins in SUOX and YedY are marked. (*C*) A zoomed-in view of superposition of *A. tumefaciens* (orange, 7kou) and *K. pneumoniae* (pink, 7rkb) PruR. The neopterin and conserved residues of the pterin-binding pocket are shown as sticks. Residue sidechains are numbered according to *A. tumefaciens*. (*D*) Superposition of all observed neopterin-binding modes from crystal structures of *K. pneumoniae* (7rkb) and *V. cholerae* (7kp2). The binding pocket is represented as an electrostatic surface potential (blue-to-red, positive-to-negative charge) and neopterin as stick models. Carbons are in yellow (alternative conformation A, *V. cholerae*), gray (alternative conformation B, *V. cholerae*, 7kp2), and green (*K. pnuemoniae*, 7rkb), with oxygen in red and nitrogen in blue. (*E*) Congo Red staining by inoculating 3 μL spots of the *A. tumefaciens* wild type and Δ*pruR* harboring plasmid-borne P_{lac}-*pruR* alleles on a single ATGN-CR plate supplemented with 75 μg/mL Congo Red and 400 μM IPTG and incubated at 30 °C for 48 h. (*F*) DSS in vivo cross-linking of the *A. tumefaciens* wild type or a Δ*pruA* mutant expressing the P_{lac}-*pruR* wild-type and mutant alleles (400 μM IPTG). The blot was probed with α-PruR polyclonal antibody (1:40,000), and GAR-HRP secondary antibody, and antibody binding was detected with chemiluminescent substrate using a BioRad ChemiDoc. Nonspecific bands serve as protein loading controls.

reports on bacterial pterins is that they accumulate extracellularly, with as much as 100-fold greater pterin in the extracellular fraction as compared to associated with cells (15, 32). Among mouse gut microbiota treated with the folate pathway inhibitor sulfamethoxazole, pterin derivatives called colipterins accumulated up to 1 to 4 nM (33). The mechanism of pterin excretion has not been elucidated, but it has been reported that extracellular pterins can re-enter cells (34). The PruR protein clearly interacts with a self-produced, reduced monapterin species in the periplasm, and by extension exogenous pterins that enter the periplasm might also act as agonists or antagonists of the H_4MPt-PruR interaction. Our findings are most consistent with H_4MPt preferentially binding to PruR. However, H_4MPt is susceptible to oxidation and thus will have a relatively short half-life in the periplasm and elsewhere outside the cell (35).

PruR-DcpA Complex Formation Is Stimulated by PruA. Our cross-linking experiments revealed a PruR-DcpA complex the size of which suggests a one-to-one-stoichiometry, and that is formed less efficiently in the Δ*pruA* mutant. It is possible that the absence of the PruA-reduced pterin destabilizes PruR, either directly or through limiting its interaction with DcpA. The Δ*pruA* mutant has a dramatic phenotype in which DcpA exhibits predominantly DGC activity, equivalent to the Δ*pruR* mutant (9), so whatever remaining interaction occurs between the two proteins in the Δ*pruA* mutant is insufficient to maintain a strong DcpA PDE bias. Our analysis of the PruR control of DcpA catalytic site mutants suggests that in cells with active PruA, the PruR-DcpA interaction stimulates PDE activity and also diminishes DGC activity. We speculate this dual action may be due the reciprocal control of dimerization for the separate DGC and PDE domains of DcpA, a process known to be required for these activities in other proteins that synthesize and degrade c-di-GMP (36, 37).

The DcpA orthologs identified here show chemical and predicted structural similarity, and two residues are invariant (WX_7E, W40, and E48 in *A. tumefaciens* DcpA). AlphaFold predictions suggest that the DcpA periplasmic domain forms an unusual four-helix CACHE-type bundle (38), with overall structural similarity to the four-helix bundles in the periplasmic domains of methyl-accepting dependent chemotaxis proteins (MCPs), that impart chemotactic motility responses to certain solutes (39). Rather than interacting directly with their ligands in the periplasm, several MCPs mediate the response through interactions with periplasmic solute-binding proteins (SBPs) (40). The interaction of PruR and the DcpA periplasmic domain may share similarities with MCP-SBP interactions, with binding of the pterin fostering this interaction.

The PruR-DcpA system is strikingly analogous to the dual-function DGC-PDE MbaA in *V. cholerae*, which is regulated through the interaction of its periplasmic domain with NspS (41, 42). NspS is an SBP for polyamines and is encoded upstream of *mbaA* in the same operon. The specific type of polyamine bound by NspS can regulate its interaction with MbaA, thereby controlling the balance of DGC and PDE activities from this enzyme. *V. cholerae* synthesizes and releases norspermidine, which stimulates DGC activity through NspS-MbaA interactions, whereas other polyamines such as spermidine inhibit association with MbaA (43, 44). The polyamine response impacts c-di-GMP levels, controlling *V. cholerae* biofilm formation. Interestingly, in the absence of polyamines, NspS can bind to MbaA and weakly impacts its activity, similar to our observation here that PruR weakly binds to DcpA in the absence of its proposed H_4MPt ligand. There are multiple types of pterins produced and excreted by bacterial and eukaryotic organisms (12, 15, 33), and it is conceivable that similar to the NspS-MbaA system, the specific pterin-associated with PruR can impact its regulation of DcpA. These structurally variant pterins may act as agonists or antagonists for the PruR-H_4MPt interaction. It is also plausible that the PruR-associated pterin acts as a proxy to detect a different cue in the periplasm, such as specific redox-active compounds.

Insights into Conserved PruR-DcpA-Type Systems in Other Bacteria. Our comprehensive probing of bacterial genomes reveals a discontinuous but wide distribution of *pruR* orthologs among

four classes of the *Proteobacteria* (Fig. 5*B*). The PruR homologs we identify here are well-conserved proteins that are highly likely to be orthologous in function—they are predicted to adopt a SUOX-type fold, sharing the residues we have found to coordinate the pteridine ring and to be required for regulation. The vast majority of the *pruR* genes are immediately upstream of a gene encoding a DcpA-type periplasmic domain (5,595 unique sequence pairs out of >24,000 matches, ~44% of families represented) (Dataset S1; 16 of 5,595 are separated by elements such as insertion sequences). The periplasmic domains of these DcpA-type proteins adopt the same predicted structure and share the WX_7E motif. Given the remarkable similarity of the PruR proteins, it is highly likely that they bind the same or related pterin ligands and provide pterin-dependent control through interaction with the DcpA-type periplasmic domain.

Many of the proteins with DcpA-like periplasmic domains have cytoplasmic domains with c-di-GMP-related functions (~71% of the total unique regulatory pairs) that are highly likely to modulate pools of this second messenger. In *A. tumefaciens,* the PruR-DcpA system regulates adhesive polysaccharide production and biofilm formation, but c-di-GMP effectors, their target functions, and relative sensitivities are quite diverse across the *Proteobacteria* (4). Although adhesion is a common target function, each bacterial strain can be tuned in different ways to its c-di-GMP pools. For a portion of the conserved *pruR-dcpA* operons, only one of the c-di-GMP functions is retained. For example, there are two of these conserved operons in *V. cholerae*, VC1933-VC1934 and VCA0075-VCA0074 [VCA0074 is the well-studied DGC known as CdgA, (45)]. Interestingly, VC1934 is unlikely to be active for c-di-GMP synthesis (due to its nonfunctional GADEF motif) but active for its degradation, and CdgA is well established to be active for c-di-GMP synthesis (45). In combination they may provide similar, but independently regulated DGC/PDE activities, as does the dual functionality of DcpA in *A. tumefaciens.* In the two major model strains of *P. aeruginosa*, PA01 and PA14, mutants for their *dcpA* homologs (PA2780/PA1426970), both impact c-di-GMP-dependent phenotypes, although to different extents (46, 47).

Additionally, our analysis revealed a large, subfamily of PruR-linked regulators we have designated the PruR-DTB systems (~29% of the total unique sequences, Dataset S1) that have the DcpA-like periplasmic module, but the cytoplasmic output domain is similar to a two-component-type TorS and BaeS histidine kinase domains (25, 26). Interestingly, in *E. coli* TorS activity is regulated by a periplasmic protein called TorT, which binds to trimethylamine (TMAO), controlling expression of genes for TMAO utilization through the TorR response regulator (26, 48). *E. coli* lacks a PruR ortholog and although TorT is an SBP, it does not resemble PruR. It is possible that the PruR-DTB systems are also integrated with c-di-GMP, but it is more likely that they are entirely distinct in their outputs. Frequently, the PruR-DTB gene clusters are proximal to two-component-type response regulator genes, perhaps providing a more canonical two-component-type transduction mechanism similar to that through TorR.

Both the PruR-DcpA and PruR-DTB subgroups are widely distributed in the APB, although notably absent from obligate intracellular bacterial families (e.g., *Rickettsiaceae*) and multiple other well-studied groups (e.g., *Caulobacteriaceae*). Even closely related APB such as *Sinorhizobium meliloti* and *A. tumefaciens* can differ in whether they have the PruR-based systems. In the GBP, these systems are predominantly found in families on two of the main lineages that have been heavily sequenced (Fig. 5*B*). PruR-based systems span the entire BPB branch of Proteobacteria, but are found in only 40% of the families and are dominated by the PruR-DTB group. Although our *A. tumefaciens* C58 study system only has one PruR-based system, it is not uncommon to identify multiple PruR-DcpA and PruR-DBT gene clusters in a single bacterial genome, and several taxa have as many as four (Dataset S1, e.g., *Aeromonas* species). For the systems with multiple models, these can all be PruR-DcpA types, all PruR-DBT types, or most frequently a combination of the two. The integration of these different coexisting PruR-linked regulatory modules will be an interesting area for future investigation.

Materials and Methods

Detailed descriptions of materials and methods can be found in *SI Appendix*. Bacterial strains and plasmids used in the study are detailed in *SI Appendix*, Tables S3 and S4. Molecular cloning, plasmid constructions, site-directed mutagenesis, and allelic replacements were performed by standard approaches. Media formulations, *A. tumefaciens* cultivation conditions, Congo Red staining, and biofilm assays were performed as previously published (49, 50). Protein expression and purification for antibody preparation, in vitro analysis, and structure determination utilized bacterial expression platforms and affinity chromatography. Western blotting of native and DSS-cross-linked complexes used SDS-PAGE gels and electrotransfer to nitrocellulose membranes and antibody-based detection. Crystallography and structural modeling were performed using established approaches. Chemical synthesis and validation of H_2-MPt was performed as described in *SI Appendix* and Fig. S12. Enzymatic assays (PhoA and DGC/PDE activities) and pterin binding experiments are detailed in *SI Appendix*. Phylogenetic analysis for *pruR-dcpA* loci in diverse bacterial genomes relied on an iterative hidden Markov model to identify genes encoding PruR-like proteins genetically linked to genes encoding a DcpA-like periplasmic domain.

Data, Materials, and Software Availability. The structures determined here were deposited in the Protein Data Bank with the assigned PDB codes: 7kos (*A. tumefaciens*) (51), 7kou (*A. tumefaciens 2*) (52), 7kom (*V. vulnificus*) (53), 7rkb (*K. pneumoniae*) (54), and 7kp2 (*V. cholerae*) (55). Protein diffraction data have been deposited at proteindiffraction.org. All additional experimental data are included in the article and/or supporting information.

ACKNOWLEDGMENTS. We thank Fitnat Yildiz, Seth Rubin, Vanessa Mariscal, Thomas Bernhardt, and Jon Beckwith for helpful discussions and Ramya Natarajan for technical assistance with preliminary protein purification. The IU Center for Genomics and Bioinformatics, particularly Ram Podicheti, was instrumental in comprehensive analysis of bacterial genomes for PruR-DcpA homologs. This project was supported by grants to C.F. (NIH R01 GM120337), K.D.A (NSF-CHE 2105598), and A.K.G. (NIH AI150466.). N.F. received support from the IU Genetics, Cellular and Molecular Sciences NIH Training Grant (T32 GM007757). Work by the Center for Structural Biology of Infectious Diseases was supported by HHS/NIH/NIAID contracts #HHSN272201700060C and 75N93022C00035. This research used resources of the Advanced Photon Source, a U.S. Department of Energy (DOE) Office of Science User Facility operated for the DOE Office of Science by Argonne National Laboratory under Contract No. DE-AC02-06CH11357. Use of the LS-CAT Sector 21 was supported by the Michigan Economic Development Corporation and the Michigan Technology Tri-Corridor (Grant 085P1000817). Access to LS-CAT and computational resources is facilitated by the NU Structural Biology Facility, which is supported by NCI grant P30 CA060553 of the Robert H. Lurie Comprehensive Cancer Center.

Author affiliations: [a]Department of Biology, Indiana University, Bloomington, IN 47405; [b]Department of Biochemistry, Virginia Polytechnic Institute and State University, Blacksburg, VA 24061; [c]Department of Microbiology-Immunology, Feinberg School of Medicine, Northwestern University, Chicago, IL 60611; [d]Center for Structural Biology of Infectious Diseases, Feinberg School of Medicine, Northwestern University, Chicago, IL 60611; [e]Department of Pharmacology, Feinberg School of Medicine, Northwestern University, Chicago, IL 60611; [f]Department of Chemistry, Purdue University, West Lafayette, IN 47907; and [g]Department of Medicinal Chemistry, Purdue University, West Lafayette, IN 47907

Author contributions: J.L.G., J.L.E., G.M., A.K.G., K.J.F.S., K.D.A., and C.F. designed research; J.L.G., J.L.E., N.F., K.B., G.M., L.S., N.L.I., J.R., K.D.A., and C.F. performed research; J.R. and A.K.G. contributed new reagents/analytic tools; J.L.G., J.L.E., N.F., K.B., G.M., L.S., N.L.I., A.K.G., K.J.F.S., K.D.A., and C.F. analyzed data; and J.L.G., J.L.E., K.B., G.M., N.L.I., K.J.F.S., K.D.A., and C.F. wrote the paper.

1. O. Ciofu, C. Moser, P. O. Jensen, N. Hoiby, Tolerance and resistance of microbial biofilms. *Nat. Rev. Microbiol.* **20**, 621–635 (2022).
2. K. Sauer *et al.*, The biofilm life cycle: Expanding the conceptual model of biofilm formation. *Nat. Rev. Microbiol.* **20**, 608–620 (2022).
3. C. Berne, C. K. Ellison, A. Ducret, Y. V. Brun, Bacterial adhesion at the single-cell level. *Nat. Rev. Microbiol.* **16**, 616–627 (2018).
4. U. Jenal, A. Reinders, C. Lori, Cyclic di-GMP: Second messenger extraordinaire. *Nat. Rev. Microbiol.* **15**, 271–284 (2017).
5. T. E. Randall *et al.*, Sensory perception in bacterial cyclic diguanylate signal transduction. *J. Bacteriol.* **204**, e0043321 (2022).
6. M. A. Thompson, M. C. Onyeziri, C. Fuqua, Function and regulation of *Agrobacterium tumefaciens* cell surface structures that promote attachment. *Curr. Top. Microbiol. Immunol.* **418**, 143–184 (2018).
7. S. B. Gelvin, *Agrobacterium*-mediated plant transformation: The biology behind the "gene-jockeying" tool. *Microbiol. Mol. Biol. Rev.* **67**, 16–37 (2003).
8. J. E. Heindl *et al.*, Mechanisms and regulation of surface interactions and biofilm formation in *Agrobacterium*. *Front. Plant Sci.* **5**, 176 (2014).
9. N. Feirer *et al.*, A pterin-dependent signaling pathway regulates a dual-function diguanylate cyclase-phosphodiesterase controlling surface attachment in *Agrobacterium tumefaciens*. *mBio* **6**, e00156 (2015).
10. J. Xu *et al.*, Genetic analysis of *Agrobacterium tumefaciens* unipolar polysaccharide production reveals complex integrated control of the motile-to-sessile switch. *Mol. Microbiol.* **89**, 929–948 (2013).
11. M. Labine *et al.*, Enzymatic and mutational analysis of the PruA pteridine reductase required for pterin-dependent control of biofilm formation in *Agrobacterium tumefaciens*. *J. Bacteriol.* **202**, e00098-20 (2020), 10.1128/JB.00098-20.
12. N. Feirer, C. Fuqua, Pterin function in bacteria. *Pteridines* **28**, 23–36 (2017).
13. J. M. Green, B. P. Nichols, R. G. Matthews, "Folate biosynthesis, reduction and polyglutamylation" in *Escherichia coli and Salmonella: Cellular and Molecular Biology*, F. C. Neidhardt, Ed. (ASM Press, Washington, D.C., 1996), vol. 1, pp. 665–673, chap. 41.
14. S. Leimkuhler, M. M. Wuebbens, K. V. Rajagopalan, The history of the discovery of the molybdenum cofactor and novel aspects of its biosynthesis in bacteria. *Coord. Chem. Rev.* **255**, 1129–1144 (2011).
15. A. Pribat *et al.*, FolX and FolM are essential for tetrahydromonapterin synthesis in *Escherichia coli* and *Pseudomonas aeruginosa*. *J. Bacteriol.* **192**, 475–482 (2010).
16. G. J. Workun, K. Moquin, R. A. Rothery, J. H. Weiner, Evolutionary persistence of the molybdopyranopterin-containing sulfite oxidase protein fold. *Microbiol. Mol. Biol. Rev.* **72**, 228–248 (2008).
17. C. Kisker *et al.*, A structural comparison of molybdenum cofactor-containing enzymes. *FEMS Microbiol. Rev.* **22**, 503–521 (1998).
18. V. R. Sokya, W. Pfleiderer, R. Prewo, Pteridines: Synthesis and characteristics of 5,6-dihydro-6-(1,2,3-trihydroxypropyl)pteridines: Covalent intramolecular adducts. *Helv. Chim. Acta.* **73**, 808–826 (1990).
19. C. Manoil, J. J. Mekalanos, J. Beckwith, Alkaline phosphatase fusions: Sensors of subcellular location. *J. Bacteriol.* **172**, 515–518 (1990).
20. H. Nielsen, K. D. Tsirigos, S. Brunak, G. von Heijne, A brief history of protein sorting prediction. *Protein J.* **38**, 200–216 (2019).
21. S. Okuda, H. Tokuda, Lipoprotein sorting in bacteria. *Annu. Rev. Microbiol.* **65**, 239–259 (2011).
22. D. Huber *et al.*, Use of thioredoxin as a reporter to identify a subset of Escherichia coli signal sequences that promote signal recognition particle-dependent translocation. *J. Bacteriol.* **187**, 2983–2991 (2005).
23. C. F. Schierle *et al.*, The DsbA signal sequence directs efficient, cotranslational export of passenger proteins to the *Escherichia coli* periplasm via the signal recognition particle pathway. *J. Bacteriol.* **185**, 5706–5713 (2003).
24. I. Letunic, P. Bork, Interactive Tree Of Life (iTOL) v5: An online tool for phylogenetic tree display and annotation. *Nucleic Acids Res.* **49**, W293–W296 (2021).
25. S. K. Leblanc, C. W. Oates, T. L. Raivio, Characterization of the induction and cellular role of the BaeSR two-component envelope stress response of *Escherichia coli*. *J. Bacteriol.* **193**, 3367–3375 (2011).
26. C. Jourlin, A. Bengrine, M. Chippaux, V. Mejean, An unorthodox sensor protein (TorS) mediates the induction of the tor structural genes in response to trimethylamine N-oxide in *Escherichia coli*. *Mol. Microbiol.* **20**, 1297–1306 (1996).
27. L. Loschi *et al.*, Structural and biochemical identification of a novel bacterial oxidoreductase. *J. Biol. Chem.* **279**, 50391–50400 (2004).
28. J. A. Ronau *et al.*, A conserved acidic residue in phenylalanine hydroxylase contributes to cofactor affinity and catalysis. *Biochemistry* **53**, 6834–6848 (2014).
29. C. Chen *et al.*, Structural basis for molecular recognition of folic acid by folate receptors. *Nature* **500**, 486–489 (2013).
30. A. S. Wibowo *et al.*, Structures of human folate receptors reveal biological trafficking states and diversity in folate and antifolate recognition. *Proc. Natl. Acad. Sci. U.S.A.* **110**, 15180–15188 (2013).
31. R. L. Blakley, S. J. Benkovic, *Folates and Pterins: Chemistry and Biochemistry of Pterins* (John Wiley & Sons Inc, 1985), vol. 2.
32. K. Iwai, M. Kobashi, H. Fujisawa, Occurrence of *Crithidia* factors and folic acid in various bacteria. *J. Bacteriol.* **104**, 197–201 (1970).
33. H. B. Park *et al.*, Sulfamethoxazole drug stress upregulates antioxidant immunomodulatory metabolites in *Escherichia coli*. *Nat. Microbiol.* **5**, 1319–1329 (2020).
34. A. Noiriel, V. Naponelli, G. G. Bozzo, J. F. Gregory III, A. D. Hanson, Folate salvage in plants: Pterin aldehyde reduction is mediated by multiple non-specific aldehyde reductases. *Plant J.* **51**, 378–389 (2007).
35. T. Arai *et al.*, Auto-oxidation of 5,6,7,8-tetrahydroneopterin. *Pteridines* **9**, 26–28 (1988).
36. C. Chan *et al.*, Structural basis of activity and allosteric control of diguanylate cyclase. *Proc. Natl. Acad. Sci. U.S.A.* **101**, 17084–17089 (2004).
37. F. Rao, Y. Yang, Y. Qi, Z. X. Liang, Catalytic mechanism of cyclic di-GMP-specific phosphodiesterase: A study of the EAL domain-containing RocR from *Pseudomonas aeruginosa*. *J. Bacteriol.* **190**, 3622–3631 (2008).
38. J. Jumper *et al.*, Highly accurate protein structure prediction with AlphaFold. *Nature* **596**, 583–589 (2021).
39. A. Ortega, I. B. Zhulin, T. Krell, Sensory repertoire of bacterial chemoreceptors. *Microbiol. Mol. Biol. Rev.* **81**, e00033–17 (2017).
40. J. P. Cerna-Vargas, B. Sanchez-Romera, M. A. Matilla, A. Ortega, T. Krell, Sensing preferences for prokaryotic solute binding protein families. *Microb. Biotechnol.* **16**, 1823–1833 (2023).
41. A. A. Bridges, J. A. Prentice, C. Fei, N. S. Wingreen, B. L. Bassler, Quantitative input-output dynamics of a c-di-GMP signal transduction cascade in *Vibrio cholerae*. *PLoS Biol.* **20**, e3001585 (2022).
42. E. Karatan, T. R. Duncan, P. I. Watnick, NspS, a predicted polyamine sensor, mediates activation of *Vibrio cholerae* biofilm formation by norspermidine. *J. Bacteriol.* **187**, 7434–7443 (2005).
43. A. A. Bridges, B. L. Bassler, Inverse regulation of *Vibrio cholerae* biofilm dispersal by polyamine signals. *Elife* **10**, e65487 (2021).
44. S. R. Cockerell *et al.*, *Vibrio cholerae* NspS, a homologue of ABC-type periplasmic solute binding proteins, facilitates transduction of polyamine signals independent of their transport. *Microbiology* **160**, 832–843 (2014).
45. S. Beyhan, L. S. Odell, F. H. Yildiz, Identification and characterization of cyclic diguanylate signaling systems controlling rugosity in *Vibrio cholerae*. *J. Bacteriol.* **190**, 7392–7405 (2008).
46. D. G. Ha, M. E. Richman, G. A. O'Toole, Deletion mutant library for investigation of functional outputs of cyclic diguanylate metabolism in *Pseudomonas aeruginosa* PA14. *Appl. Environ. Microbiol.* **80**, 3384–3393 (2014).
47. K. Eilers *et al.*, Phenotypic and integrated analysis of a comprehensive *Pseudomonas aeruginosa* PAO1 library of mutants lacking cyclic-di-GMP-related genes. *Front. Microbiol.* **13**, 949597 (2022).
48. C. Baraquet *et al.*, TorT, a member of a new periplasmic binding protein family, triggers induction of the Tor respiratory system upon trimethylamine N-oxide electron-acceptor binding in *Escherichia coli*. *J. Biol. Chem.* **281**, 38189–38199 (2006).
49. E. R. Morton, C. Fuqua, Unit3D. 1 Laboratory maintenance of *Agrobacterium*. *Curr. Protoc. Microbiol.* **Chapter 1**, Unit3D.1 (2012).
50. E. R. Morton, C. Fuqua, Phenotypic analyses of *Agrobacterium*. *Curr. Protoc. Microbiol.* **Chapter 3**, Unit 3D.3 (2012).
51. G. Minasov *et al.*, 1.50 Angstroms resolution crystal structure of putative pterin binding protein PruR (Atu3496) from *Agrobacterium fabrum* str. C58. Protein Data Bank. https://www.rcsb.org/structure/7KOS. Deposited 9 November 2020.
52. G. Minasov *et al.*, 1.83 Angstroms resolution crystal structure of putative pterin binding protein PruR (Atu3496) from *Agrobacterium fabrum* str. C58. Protein Data Bank. https://www.rcsb.org/structure/7KOU. Deposited 10 November 2020.
53. G. Minasov *et al.*, High resolution crystal structure of putative pterin binding protein PruR (VV2_1280) from *Vibrio vulnificus* CMCP6. Protein Data Bank. https://www.rcsb.org/structure/7KOM. Deposited 9 November 2020.
54. G. Minasov *et al.*, Crystal structure of putative pterin binding protein (PruR) from *Klebsiella pneumoniae* in complex with neopterin. Protein Data Bank. https://www.rcsb.org/structure/7RKB. Deposited 22 July 2021.
55. G. Minasov *et al.*, High resolution crystal structure of putative pterin binding protein (PruR) from *Vibrio cholerae* O1 biovar El Tor str. N16961 in complex with neopterin. Protein Data Bank. https://www.rcsb.org/structure/7KP2. Deposited 10 November 2020.